HEFAT2010
7th International Conference on Heat Transfer, Fluid Mechanics and Thermodynamics
19-21 July 2010
Antalya, Turkey

FUNDAMENTALS OF MODELLING A TWO-PHASE REFRIGERANT HEAT EXCHANGER- AN INDUSTRIAL PERSPECTIVE

Pradeep Bansal
Department of Mechanical Engineering
The University of Auckland, Private Bag 92019
Auckland, New Zealand
(Email: p.bansal@auckland.ac.nz)

ABSTRACT

A heat exchanger is the heart of any thermal or refrigeration system, and hence its proper design is of paramount importance to industry. Modelling is an economical and efficient way to design a thermal system (and hence a heat exchanger) and predict its performance without conducting detailed time intensive and costly physical experiments. Although the physics of two 'generic' modelling techniques, namely LMTD and NTU-e, is well covered in the basic heat transfer text books, applying these techniques can be quite an involved process in some difficult situations, such as complex heat exchanger geometries, one or both streams undergoing phase change or moisture removal from an air stream, heat exchanger experiencing a 'pinch point' etc. In some situations, models can also become quite sophisticated and use more advanced techniques, where a heat exchanger involving two-phase is modelled following a segment, zone by zone or an elemental approach. An elemental method is intensive but can be comprehensive and accurate. This paper reviews some of these modelling fundamentals for a two-phase heat exchanger, and presents two novel examples of heat exchangers that were optimised for their energy efficient use in domestic refrigerators. These were well received by the industry.

INTRODUCTION

Heat exchangers are used as heat transfer devices in a variety of thermal applications, in the form of evaporators, condensers, sub-coolers, super-heaters, etc.

Some heat exchangers that deal with fluids that undergo transformation of phase can experience heat transfer in superheated, sub-cooled and two-phase zones based on the refrigerant phase. Following the First Law of Thermodynamics, the total energy lost or gained by the refrigerant equals that gained or lost by the secondary fluid. Hence the total heat transfer rate can be generalised as:

$$\dot{Q}_{HX} = \dot{Q}_r = \dot{Q}_s = \sum \dot{Q}_z \qquad (1)$$

The total heat transfer in the heat exchangers is determined according to the number of available lumped regions such as two-phase and superheated regions in evaporators and superheated, two-phase and sub-cooled regions in condensers.

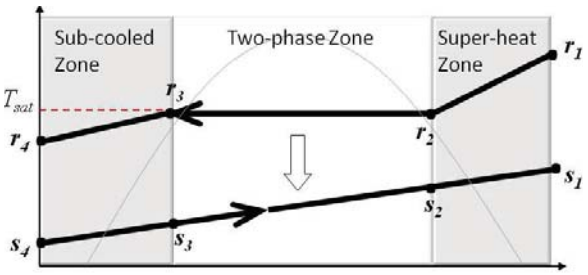

Figure 1: Three lumped zones for a condenser

Considering phase transformation occurring in a refrigerant condenser (as shown in Figure 1), the refrigerant inlet is in the super-heat zone at r_1 and is cooled to r_2, two-phase zone is between r_2 and r_3 where the temperatures or pressures do not vary with length, the refrigerant is further cooled in the sub-cooled zone to r_4 to ensure single phase at the condenser exit. The temperature and pressure for the refrigerant is normally constant in the two-phase zone, from r_3 to r_4. The heat transfer between the two fluids is summarised in Table 1, where the heat transfer rates can be separated into the three zones.

Table 1: Summary of condenser heat transfer

Zone	Refrigerant	Secondary fluid
$\dot{Q}_{sh}$	$\dot{Q}_{r1-r2} = \dot{m}_r(h_{r1} - h_{r2})$	$\dot{Q}_{s1-s2} = \dot{m}_s Cp_s(T_{s1} - T_{s2})$
$\dot{Q}_{tp}$	$\dot{Q}_{r2-r3} = \dot{m}_r(h_{r2} - h_{r3})$	$\dot{Q}_{s2-s3} = \dot{m}_s Cp_s(T_{s2} - T_{s3})$
$\dot{Q}_{sc}$	$\dot{Q}_{r3-r4} = \dot{m}_r(h_{r3} - h_{r4})$	$\dot{Q}_{s3-s4} = \dot{m}_s Cp_s(T_{s3} - T_{s4})$

MODELLING ANALOGY

The total heat transfer rate between the two fluids can be represented as the sum of heat transfer rates at each zone, as given by Equation (2). Total heat transfer in the three zones of a condenser can be given by Equations (3) and (4) for LMTD and NTU-e methods respectively. The variables for each method for the three zones are given in

Table 2.

$$\dot{Q} = \dot{Q}_{sh} + \dot{Q}_{tp} + \dot{Q}_{sc} \quad (2)$$

$$\dot{Q} = (UA)_{sh}\Delta T_{LMTD,sh} + (UA)_{tp}\Delta T_{LMTD,tp} + (UA)_{sc}\Delta T_{LMTD,sc} \quad (3)$$

$$\dot{Q} = \varepsilon_{ds}\left(\dot{Q}_{max}\right)_{ds} + \varepsilon_{tp}\left(\dot{Q}_{max}\right)_{tp} + \varepsilon_{sc}\left(\dot{Q}_{max}\right)_{sc} \quad (4)$$

Table 2: LMTD and NTU-e methods

LMTD	NTU-e
$\Delta T_{LMTD,z} = \frac{\Delta T_{1,z} - \Delta T_{2,z}}{ln\left(\frac{\Delta T_{1,z}}{\Delta T_{2,z}}\right)}$	$\dot{C}_{min,z} = min\begin{cases}\dot{C}_r = (\dot{m}Cp)_r \\ \dot{C}_s = (\dot{m}Cp)_s\end{cases}$
	$NTU_z = \frac{(UA)_z}{C_{min,z}}$
Superheat zone	
$\dot{Q}_{sh} = (UA)_{sh}\Delta T_{LMTD,sh}$	$\dot{Q}_{sh} = \varepsilon_{sh}\dot{Q}_{max,sh}$
$\Delta T_{1,sh} = T_{r1} - T_{s1}$	$\dot{Q}_{max,sh} = C_{min,sh}(T_{s4} - T_{r3})$
$\Delta T_{2,sh} = T_{r2} - T_{s2}$	$\varepsilon_{ds} = \frac{1 - \exp\left[-NTU_{sh}(1 - C_{R,sh})\right]}{1 - C_{R,sh}\exp\left[-NTU_{sh}(1 - C_{R,sh})\right]}$
	$C_{R,sh} = C_{min,sh}/C_{max,sh}$
Two-phase zone	
$\dot{Q}_{tp} = (UA)_{tp}\Delta T_{LMTD,tp}$	$\dot{Q}_{tp} = \varepsilon_{tp}\dot{Q}_{max,tp}$
$\Delta T_{1,tp} = T_{r2} - T_{s2}$	$\dot{Q}_{max,ds} = (\dot{m}Cp)_s(T_{r2} - T_{s3})$
$\Delta T_{1,tp} = T_{r3} - T_{s3}$	$\varepsilon_{ds} = 1 - \exp(-NTU_{tp})$
	$\dot{C}_{min,tp} = \dot{C}_c = (\dot{m}Cp)_s$
	$C_{R,ds} \approx 0$
Sub-cooling zone	
$\dot{Q}_{sc} = (UA)_{sc}\Delta T_{LMTD,sc}$	$\dot{Q}_{sc} = \varepsilon_{sc}\dot{Q}_{max,sc}$
$\Delta T_{1,tp} = T_{r3} - T_{s3}$	$\dot{Q}_{max,sc} = C_{min,sc}(T_{r3} - T_{s4})$
$\Delta T_{1,tp} = T_{r4} - T_{s4}$	$\varepsilon_{sc} = \frac{1 - \exp\left[-NTU_{sc}(1 - C_{R,sc})\right]}{1 - C_{R,sc}\exp\left[-NTU_{sc}(1 - C_{R,sc})\right]}$
	$C_{R,sc} = C_{min,sc}/C_{max,sc}$

The subscript z can be substituted in the generalised formulae for the three zones in both, the LMTD and NTU-e methods. A number of studies related to the subject are available in the literature [Bansal *et al* (2001), Bansal *et al* (2003a-b), Domanski and Yashar (2007), Iu *et al* (2003, 2007), Singh *et al* (2009)].

GENERAL ASSUMPTIONS

Heat exchangers are generally modelled for a steady state, steady flow conditions. This generally suggests that the mass flow rate does not vary along the heat exchanger length. Convective heat transfer coefficient for single phase flow is considered constant through the length of the heat exchanger. In the two-phase zone, the refrigerant is assumed to have constant temperature, while convective heat transfer coefficient is a function of refrigerant vapour quality. In this zone, the secondary fluid does not experience phase change, while frosting is assumed to occur over time on the surface of evaporators.

OVERALL HEAT TRANSFER COEFFICIENT

The overall heat transfer coefficient of a heat exchanger, U, is based on the internal and external heat transfer coefficients, wall resistance, frost resistance, contact resistance and fouling factors of the heat exchangers. Generally, the largest resistance determines the overall heat transfer.

$$R_{tot} = \frac{1}{UA} = \sum_{i=1}^{n} R_i \quad (5)$$

where n depends on the heat exchanger geometry and application. Some the resistances that can contribute in condensers and evaporators include:

$$R_1 = \frac{1}{\eta_i \alpha_i A_i}$$ *Internal conductive resistance*

$$R_2 = \frac{1}{\eta_o \alpha_o A_o}$$ *External conductive resistance*

$$R_3 = \frac{R_{f,i}}{\eta_i A_i}$$ *Internal fouling resistance*

$$R_4 = \frac{R_{f,o}}{\eta_o A_o}$$ *External fouling resistance*

$$R_5 = \frac{\Delta x}{kA}$$ *Conductive plain wall resistance*

$$R_5 = \frac{ln\,(d_o/d_i)}{2\pi kL}$$ *Conductive tubular resistance*

The inner tube in a tube-in-tube heat exchanger has fluid interaction on the exterior and interior surfaces of its wall. Thus convective resistances, along with fouling, must include both sides of the wall. Only one factor for conduction between the walls contributes to the total resistance. For a tubular heat exchanger, the tube wall resistance is used.

Surface efficiencies, η, are incorporated to account for enhancements to the tube surface. For a smooth un-finned surface, η=1.

Frost on heat exchanger surface

As reported by Getu and Bansal (2006, 2007), an evaporator may include additional resistances that account for frost formation. As frost builds up, this resistance constantly varies with time.

$$R_6 = \frac{t_{frost}}{k_{frost}\varphi_o} \quad (6)$$

The thermal resistance of frost layer relies on the thickness and conductivity of the frost layer, which in turn, rely on the frost density. The frost density can be evaluated using empirical correlations of Tao et al. (1993) with the temperature difference between the water triple point and evaporator coil surface. The thermal conductivity of the frost can be determined from Seker et al. (2004) correlation, which is a function of frost density.

The overall heat exchanger efficiency, φ_o, for both dry and frosted coils can be given as:

$$\varphi_o = 1 - \frac{A_f}{A_T}(1 - \varphi_f) \quad (7)$$

For fins that are circular with insulated tips, the fin efficiency, φ_f, can be calculated analytically as:

$$\varphi_f = \left(\frac{2r_0}{mr_f(r_0 + r_f)}\right)\frac{I_1(mr_f)K_1(mr_o) - K_1(mr_f)I_1(mr_o)}{I_0(mr_0)K_1(mr_f) + K_0(mr_0)I_1(mr_f)} \quad (8)$$

where

$$m = \left[\frac{2(\alpha_a - \alpha_{lat})}{k_{frost}t_{frost}}\right]^{0.5} \quad (9)$$

and I_0 and K_0 are the modified zero-order Bessel functions of the first and second kinds, respectively whereas I_1 and K_1 are the modified first-order Bessel functions of the first and second kinds, respectively.

The rate of frost accumulation on the evaporator surface is determined from equation (10), and the mass of the frost accumulated on evaporator surfaces for each time step Δt can be obtained by equation (11).

$$\dot{m}_{frost} = \dot{m}_a(\omega_{ave} - \omega_s) \quad (10)$$

$$\Delta m_{frost} = \dot{m}_{frost}\Delta t \quad (11)$$

where the frost thickness Δt_{frost} for this time step is then calculated by:

$$\Delta t_{frost} = \frac{\Delta m_{frost}}{A_{e,tp}\,\rho_{frost}} \quad (12)$$

These are added to the frost mass and thickness of previous time steps in an accumulative manner to determine the overall frost mass and thickness. The thickness of the frost increases until the start of the defrosting period. This analysis has been extended further in a separate section on "Evaporator frost formulation" later in the paper.

SINGLE-PHASE FLOW

A fluid (i.e. a refrigerant) is in single-phase when it is in the sub-cooled (*sc*) or the super-heated (*sh*) state. LMTD and NTU-e interpretations for these zones are shown in

Table 2, where the effectiveness and NTU relation is for a counter flow, tubular heat exchanger. It is assumed that the secondary fluid does not change phase and hence is in single phase through the length of the heat exchanger.

Single-phase refrigerant and secondary fluid heat transfer coefficients can be calculated from the specific flow regimes i.e., laminar or turbulent. The correlations for turbulent flow regimes can be obtained from Petukhov's correlation [Chapman (1984)]:

$$Nu_D = \frac{\alpha D}{k} = \left(\frac{f}{8}\right)\left(\frac{Pr_D}{1.07 + 12.7(f/8)(Pr_D{}^{2/3} - 1)}\right)\left(\frac{\mu}{\mu_s}\right)^n \quad (13)$$

where the friction factor is calculated as:

$$f = ((1.82\,log\,Re_D) - 1.64)^{-2} \quad (14)$$

and the constant, n, applies for the following conditions-

$n = 0.11$ for liquids, $t_s > t_b$,
$n = 0.25$ for liquids, $t_s < t_b$,
$n = 0$ for gases,
$0.5 < Pr_D < 2000$ and $10^4 < Re_D < 5x10^6$,
$0 < \mu/\mu_s < 40$, μ_s is calculated at t_s, whereas the other refrigerant properties are determined at t_b.

For turbulent flows with:

$Re_D \geq 10^6$, $2000 \leq Pr_D \leq 16700$, *and* $L/D \geq 10$, Sieder and Tale's correlation from Incropera and DeWitt (1990) is used to calculate the Nusselt number:

$$Nu_D = 0.027Re_D{}^{4/5}Pr_D{}^{1/3}\left(\frac{\mu}{\mu_s}\right) \quad (15)$$

For critical and transition flow regimes with:

$2300 \leq Re_D \leq 4000$ and $0.5 \leq Pr_D \leq 2000$, Gnielinski' correlation from Incropera and DeWitt (1990) is used to determine the Nusselt number.

$$Nu_D = \frac{(f/8)(Re_D - 1000)Pr_D}{1 + 12.7(f/8)^{1/2}(Pr_D{}^{2/3} - 1)} \quad (16)$$

where, the friction factor f is given by:

$$f = (0.79\,ln(Re_D) - 1.64)^{-2} \quad (17)$$

For fully developed laminar flow with a constant tube surface temperature, Chapman (1984) correlation is used to calculate the Nusselt number:

$$Nu_D = 3.66 \quad (18)$$

TWO-PHASE FLOW

The two-phase zone (*tp*) experiences no temperature change for the refrigerant, thus, the temperature difference for the heat transfer fluid is observed for the heat transfer in the LMTD method. The temperatures at stages 2 and 3 in Figure 1 are at saturation temperature of the refrigerant. The specific heat of a

fluid is inversely proportional to its temperature change. For this reason, the capacitance of the heat transfer fluid is the minimum capacitance. This also implies to the effectiveness of the heat exchanger at this zone, the capacitance ratio is zero.

The heat transfer coefficient of single-phase $\alpha_{o,tp}$ fluid can be calculated using the single phase heat transfer correlations. For two-phase condensation within horizontal tubes, Collier and Thome (1994) have presented a modified correlation of Dittus-Boelter correlation as:

$$\alpha_{i,tp} = \frac{C Re_D{}^n Pr_f{}^{1/2} k_{fluid}}{d_{i,tp}} \quad (19)$$

where the equivalent Reynolds number ($Re_D = DG_e/\mu$) for two-phase flow is calculated for an equivalent mass flux, defined as:

$$G_e = G\left[(1-x) + x\left(\frac{\rho_l}{\rho_v}\right)^{0.5}\right] \quad (20)$$

and
$C = 0.0265$ and $n = 0.8$ *for* $Re_D > 50{,}000$
$C = 5.03$ and $n = 1/3$ *for* $Re_D < 50{,}000$

The flow pattern maps can also be implemented to determine the heat transfer coefficients of the refrigerant. Studies have shown that heat transfer correlations based on flow pattern maps give the most accurate heat transfer coefficients.

AIR-SIDE HEAT TRANSFER COEFFICIENTS AND PRESSURE DROP

The air-side convective heat transfer coefficients are determined following the correlations of Kim et al. (1998), which employ the Colburn-*j* factor. The value of *j* for a heat exchanger having three or more tube rows in the direction of air. Here, the Reynolds number, Re_D, is determined at the minimum flow area.

Depending on the number of tube rows, the convective heat transfer coefficient is then calculated by:

$$\alpha_a = jCp_{ma}\frac{G_{ma}}{Pr_D{}^{2/3}} \quad (21)$$

The friction factors for tube bank and fins of the heat exchangers are combined to calculate the total friction factor following Kim et al. (1998). Using the combined friction factor, the pressure drop over the evaporator is estimated from Kays and London (1964).

$$\Delta P = \frac{G_{max}{}^2}{2\rho_{air}}\left[(1+\sigma^2)\left(\frac{\rho_{air,i}}{\rho_{air,o}} - 1\right) + f\frac{A_T}{A_f}\left(\frac{\rho_{air,i}}{\rho_{air,i}+\rho_{air,o}}\right)\right] \quad (22)$$

EVAPORATOR FROST FORMATION

When the surface temperature of evaporator coils falls below 0^0C, water vapour in the air condenses forming frost on the coils. Large frost accumulation decreases the performance of the coil by reducing the flow of air and increasing the thermal resistance. This results in the reduction of refrigeration capacity of the evaporator. The rate of heat gain due to the mass transfer associated with the dehumidification of the air is calculated from a latent convective heat transfer coefficient of the air, as proposed by Threlkeld (1970).

Total heat transfer rate in a heat exchanger is the sum of the heat transfer rates in different zones as given in equation (1). Rates of heat transfer of the refrigerant and secondary fluid are as given in Table 1. In the case of an evaporator, where the secondary fluid is generally air, the sum of heat transfer in the two-phase and superheat zones equates to the total heat transfer.

The latent heat transfer rate in the two-phase region of the evaporator is given by Getu and Bansal (2006) as:

$$\dot{Q}_{e,lat} = \alpha_{lat}(T_{e,air,ave} - T_s)A_{e,tp} \quad (23)$$

and the sensible rate of heat transfer in the two-phase region of the evaporator is:

$$\dot{Q}_{e,sen} = \alpha_a(T_{e,air,ave} - T_s)A_{e,tp} \quad (24)$$

The latent heat transfer coefficient is determined by:

$$\alpha_{lat} = \frac{\alpha_a \alpha_{sg}(\omega_{ave} - \omega_s)}{LeCp(T_{e,air,ave} - T_s)} \quad (25)$$

where the air/frost interface humidity ratio, ω_s, is calculated as a function of T_s, atmospheric pressure and the relative humidity of the air leaving the evaporator; and the Lewis number, L_e, is assumed to be 1.

The average evaporator air temperature and humidity ratios are respectively given by equations (26) and (27).

$$T_{e,air,ave} = T_{e,air,o} + \frac{T_{e,air,sp} - T_{e,ref,i}}{ln\left(\frac{T_{e,air,sp} - T_{e,ref,i}}{T_{e,air,o} - T_{e,ref,i}}\right)} \quad (26)$$

$$\omega_{ave} = \frac{\omega_i + \omega_o}{2} \quad (27)$$

The sublimation latent heat, h_{sg}, is estimated from the correlation reported by Ismail and Salinas (1999):

$$\alpha_{sg} = 2322(-0.04667(1.8T_s + 32) + 1220.1) \quad (28)$$

The air/frost interfacial temperature, T_s, is iteratively calculated by:

$$T_s = T_{e,air,ave} - \frac{\dot{Q}_{e,tp}}{(h_a + h_{lat})A_{e,tp}} \quad (29)$$

DIFFERENCES BETWEEN LMTD AND $NTU - \varepsilon$ APPROACHES

LMTD is normally applied when both inlet and outlet conditions are known and heat exchanger size is to be determined, while $NTU - \varepsilon$ method is used to predict the heat exchanger performance and to find the outlet conditions. However, LMTD is a lumped modeling approach, where global

UA for the whole heat exchanger is defined. Hence, more advanced modeling techniques (see proceeding section) can't be applied in the LMTD approach within each of the three zones since neither the heat transfer rates nor the outlet conditions are known in such situations. Therefore, $NTU - \varepsilon$ approach is normally applied since the convective heat transfer coefficient can be a function of refrigerant quality as the model marches along each element along the length of the heat exchanger, yielding more accurate results.

MODELLING TECHNIQUES USING $NTU - \varepsilon$ APPROACH

Vapour compression cycle based refrigeration and/or heat pump systems are commonly used for both heating and cooling purposes worldwide, where evaporator and condenser are two most important parts of the system. Appropriate design for the size of these heat exchangers is always a contentious issue, where simulation models provide useful information about the effect of various parameters on its effectiveness.

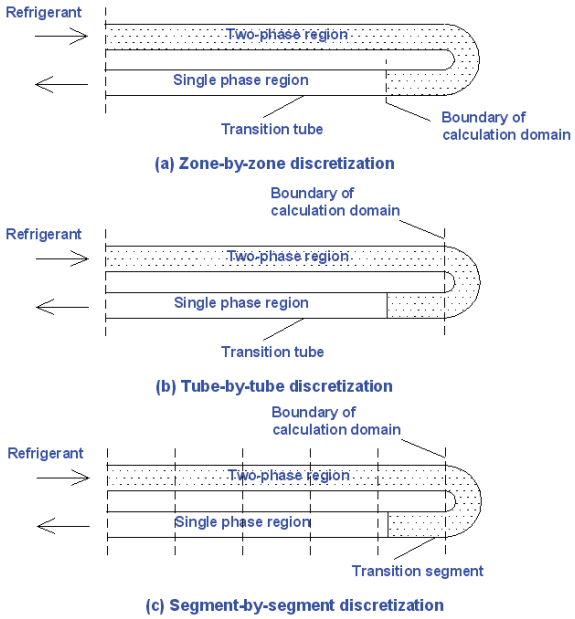

Figure 2: Discrete heat exchanger models

There are a variety of heat exchanger models available in the open literature that can be classified into three categories, namely zone-by-zone (ZZ), tube-by-tube (TT) and segment-by-segment (SS) models. These are shown in Figure 1. Both the tube-by-tube and the segment-by-segment models are sufficiently detailed to accommodate heat exchanger circuit design. Zone-by-zone (ZZ) models the heat exchanger into "zones", which are defined according to the state of the refrigerant, i.e. superheated, two-phase and/or sub-cooled.

Tube-by-tube (TT) models define each single tube in the heat exchanger as a calculation domain. Each tube is treated as an isolated heat exchanger and calculated one-by-one along the refrigerant flow direction until the coil outlet is reached. Constant refrigerant properties are assumed throughout each tube. The air side boundary condition for each tube is obtained from the calculation results of the upstream tubes. These models require considerably more computation time than the ZZ models. However, segment-by-segment (SS) models define a small segment of a single heat exchanger tube in the calculation. The calculation procedure is the same as the tube-by-tube model, but both the accuracy and the computation time are higher.

Elemental or SS heat exchanger models [Browne and Bansal (2001) and Getu and Bansal (2006)] are increasingly used in the design calculations of refrigeration/heat pump systems because of their ability to accurately model complex heat exchanger circuits and non-uniform coil face velocities. These models usually assume that refrigerant properties are constant in each element.

Elemental model

In order to determine the conditions along the length of a heat exchanger, condenser or evaporator model can be developed using finite element and variable conductance approach as shown in Figure 3. The schematics and elemental unit is able to model the performance of a heat exchanger at various positions along its length. Elemental model can be implemented within the all zones and is based on the NTU-e method. In the two-phase zone, it can account for the change of heat transfer coefficients with vapour quality.

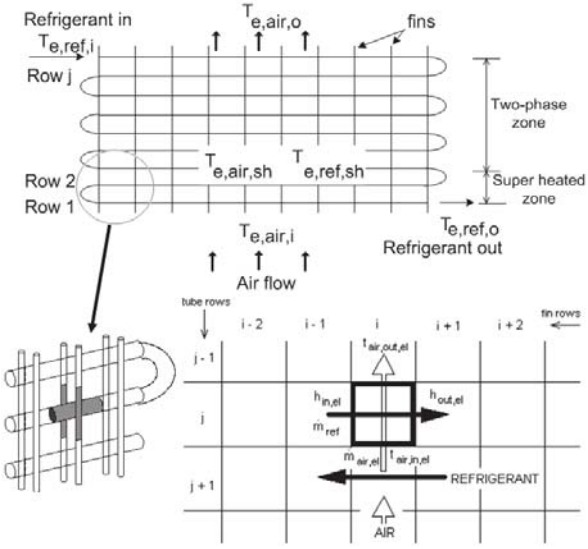

Figure 3: Typical schematic of an elemental unit of a typical heat exchanger (see Figure 7 for detailed condenser)

The calculated steady state outlet conditions from previous elements are used as the inlet conditions of adjacent elements. The vapour quality of an element, which is needed in the calculation of the refrigerant heat transfer coefficient in two-phase zone, is determined from the element's enthalpy. Calculation of properties in each element of the matrices can be carried out independently of each other and, depending on the element's quality; the equations for single-phase or two-phase heat transfer are solved. An iterative subroutine method can be employed to find the heat transfer rates for each element. Subroutines used by Bansal et al. (2001, 2003a, 2003b) for the elemental analysis of an evaporator and condenser calculate the heat transfer rates by summing the heat transfer for each row (i) and column (j) for each layer (l) as below:

$$\dot{Q}_e = \sum_{elements} \dot{Q}_z = \sum_{l=1}^{N_l} \left[\sum_{j=1}^{N_j} \left(\sum_{i=1}^{N_i} \dot{Q}_{element}(j,i) \right) \right] \quad (30)$$

where the overall heat transfer coefficient for each element is described as:

$$UA_{HX} = \sum_{elements} UA_z = \sum_{l=1}^{N_l} \left[\sum_{j=1}^{N_j} \left(\sum_{i=1}^{N_i} UA_{element}(j,i) \right) \right] \quad (31)$$

CASE STUDIES

Egg crate (or Corrugated) evaporator

'Egg-crate' type evaporators (shown in Figure 4) are forced flow evaporators developed for domestic refrigerators/freezers. These evaporators are cheap, easy to produce, are manufactured in various sizes, and have high efficiency. They are made of aluminium, having continuous rows of rectangular fins where the fin layers are press fitted onto the serpentine bent evaporator tube. These evaporators work in counter/parallel-cross flow configuration with refrigerant R134a as the working fluid. Bansal et al. (2001) developed a model of these evaporators that describes the steady state heat transfer performance of the evaporator and uses the NTU-e method following an elemental approach as mentioned previously. The model accounts for the refrigerant pressure drop inside the tubes, which leads to a temperature change of the refrigerant along the tube during the evaporation process.

To validate the model, test data was collected from an experimental test rig as shown in 5. The test section consisted of a closed loop duct (wind tunnel) that housed the test evaporator and relevant instrumentation. The duct was integrated inside a big chest freezer that delivered constant air temperatures of about –15 °C. Constant temperature distribution had been reached by using a fan to mix and move the air in the outer chest freezer. The duct walls consisted of high-density plastic and were insulated with 40-60 mm thick polystyrene. The corners of the duct were round shaped to minimize the flow resistance in these zones. The test evaporator inside the duct was connected with its own separate refrigerant circuit outside the chest freezer. Inside the wind tunnel, the air was circulated by a fan situated upstream of the evaporator.

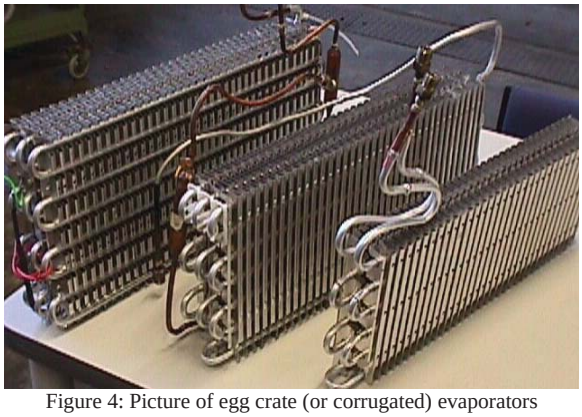

Figure 4: Picture of egg crate (or corrugated) evaporators

After flowing over the evaporator, the cold air passed over an electric resistance heater, which heated up the air to a desired temperature. A power transducer measured the electrical energy supplied to both the heater and the fan in the duct. An upstream mixing chamber maintained the airflow in the duct. The mixing chamber consisted of two plates, 20 cm apart. A number of small holes were distributed over the plate surface to mix the airflow. In the middle of each mixing chamber, three temperature probes (left, middle, right) were installed in line to each other. Four other temperature probes were situated in each corner of the duct to control the temperature distribution of the circulating air. Refrigerant temperatures were measured at the inlet and outlet of the evaporator. Refrigerant left the evaporator almost saturated during all tests (i.e. no superheat). The refrigerant mass flow rate was not measured in the experiments but was calculated from the air energy balance. The flow rate was compared with the values from the compressor performance data at operating evaporator temperatures and pressures and the two values were found to be close. The temperature measurements in the rig were all taken with Analog temperature devices (ATD's). An ATD is considered to be a more accurate device that works on the principle of resistance thermometry. The maximum measurement uncertainty of this type of ATD was 0.1°C in the temperature range from –25 °C to 105 °C, and they were calibrated in an ice bath. Air inlet temperatures ranged from –9 to –18 °C while the refrigerant temperatures were in range of –18 to -26°C. Airflow rates were measured using a hot wire anemometer. The certified measurement accuracy was ±5.0 % of the reading in the range from 0 to 20 m/s. Air velocities of the tests ranged from 0.47 to 0.82 m/s depending on the fan frequency. No measurements could specifically be made for fan power. The test data were collected at one-minute intervals over a period of 8 to 24 hours from the beginning to the end of the tests.

It may be inferred that the air-side (outside) heat transfer co-efficient (α_o) increases monotonically with the Reynolds number but decreases with both the hydraulic diameter (D_h) and the finning factor (η). Also, Reynolds number is inversely proportional to the minimum flow area (A_{min}). Therefore, for improved evaporator design, the influence of the fin parameters (fin density, fin height, fin thickness) was assessed individually on the evaporator performance. The base parameters of the present staged evaporator design (i.e. tube diameter, longitudinal tube pitch, number of tubes rows, number of fins layers, fin layer width etc.) were unchanged. Other base inputs to the model included: Air velocity varying between 0.4 and 0.8 m/s, temperatures of air and refrigerant at evaporator inlet being -13^{o}C and -20^{o}C respectively, refrigerant mass flow rate of 0.0015 kg/s, and refrigerant quality at the evaporator inlet of 0.2.

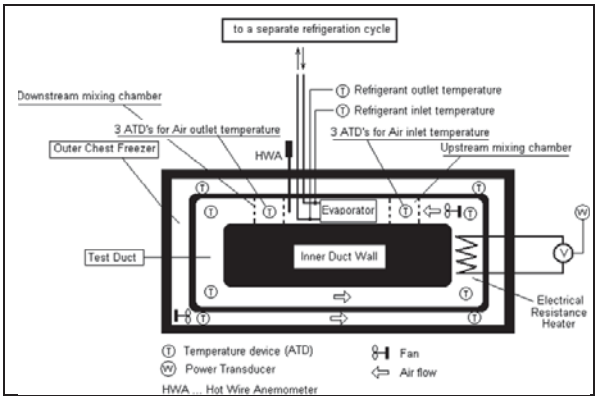

Figure 5: Experimental rig to test the egg crate evaporators

The hydraulic diameter has been used as the global variable in this study to visualise the effect of individual fin parameters on the evaporator performance. Since hydraulic diameter decreases with fin density, increasing fin density leads to decreased A_{min} and hence increased Reynolds numbers for the given air flow rate. The resulting effect on α_o (or h_o in Fig. 6), UA and evaporator capacity can be seen in Figure 6. α_o increases marginally while both the UA and the evaporator capacity increase appreciably with fin density.

Similar results can be observed for fin height. Increasing the fin height results in an increase in hydraulic diameter, minimum flow area and fin factor. As the minimum flow area increases, the Reynolds number decreases and consequently, the outside heat transfer coefficient decreases. The hydraulic diameter is an important parameter in the heat transfer behaviour of the evaporator. Shorter fins are better for improved heat transfer but they lead to increased airside pressure drop.

The general trend shows that thicker fins result in decreased D_h and lead to increased outside heat transfer, increasing both the UA-value and the evaporator capacity. All three parameters decrease with higher hydraulic diameters (i.e. for thinner fins) but improve with higher airflow rates.

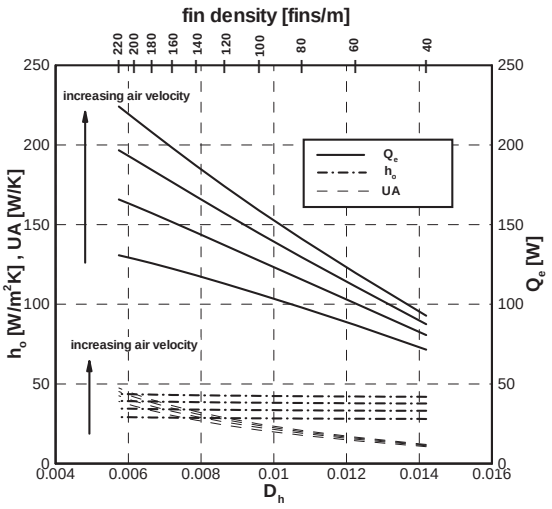

Figure 6: Evaporator capacity, outside heat transfer co-efficient, and UA versus hydraulic diameter for varying fin density

Wire and tube condenser

One of the commonly used condensers in domestic refrigerators is the wire-and-tube condenser. The wire-and-tube condenser is predominantly a natural convection heat exchanger. It consists of a single copper tube and solid steel wires that serve as extended surfaces. The tube which carries the refrigerant is bent into a single-passage serpentine shape with wires symmetrically attached to both sides in a direction normal to the tubes.

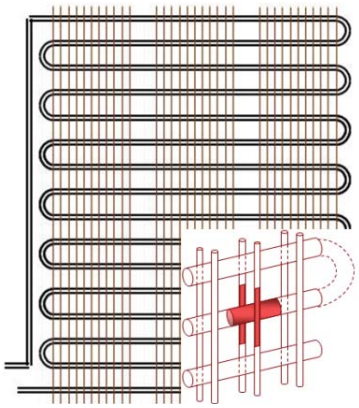

Figure 7: Wire and tube condenser (its element was shown in Figure 3)

Bansal and Chin (2003 a, 2003b) developed a computer model to analyse the performance of the condenser for different design parameter using the elemental modelling technique as aforementioned. The wire-and-tube condenser is a natural draft type heat exchanger with relatively different tube geometry and flow direction than conventional heat exchangers, and hence, a distinct model was developed for its performance.

To validate the model, experiments were conducted on a wire-and-tube condenser (as shown in Figure 7) using a refrigerator, and the experimental rig as shown in Figure 8. Closed-door experiments were carried out on a two door refrigerator in an environmental chamber, which was maintained at 20 or 25^{o}C (±0.5^{o}C) and at 55% relative humidity (±5%) for all the tests. Measurements of refrigerant temperature, pressure and mass flow rate, and power consumption by the refrigerator were taken during the experiments.

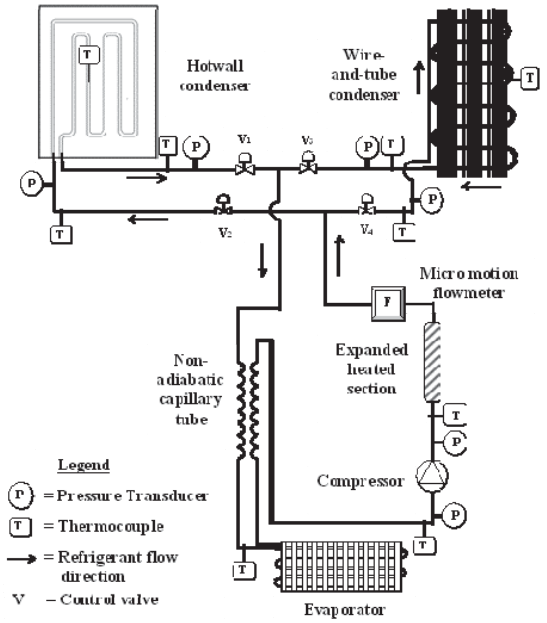

Figure 8: Experimental rig to test the condenser

The modelling results were compared with the experimental data for different saturation temperature conditions where the refrigerant was fully condensed at the condenser outlet. Results, as shown in Figure 9, have found that radiative and convective are the two heat transfer mechanisms at the outer surface of the condenser. These with the overall heat transfer coefficient were modelled for G =115 kg/s.m2 and T_{sat} =40^{o}C.

At the superheated zone, the radiation heat transfer dominates the heat transfer. The inner heat transfer coefficient increases rapidly in the two-phase zone, resulting in the increase in overall heat transfer coefficient. The convective heat transfer coefficient remains almost constant along this zone. In the sub-cooled, the refrigerant temperature drops considerably. Thus, h_{conv} drops accordingly.

In general, h_{conv} depends on the both the geometry of the heat transfer area and the temperature. The overall heat transfer coefficient, U is used to compute the heat transfer using the temperature difference between the refrigerant and the ambient temperature. It exhibits similar pattern with h_{conv} as the convective heat transfer dominates the total heat transfer. The radiation heat transfer coefficient does not change significantly (at about 5.8 W/m^{2}K) across the condenser.

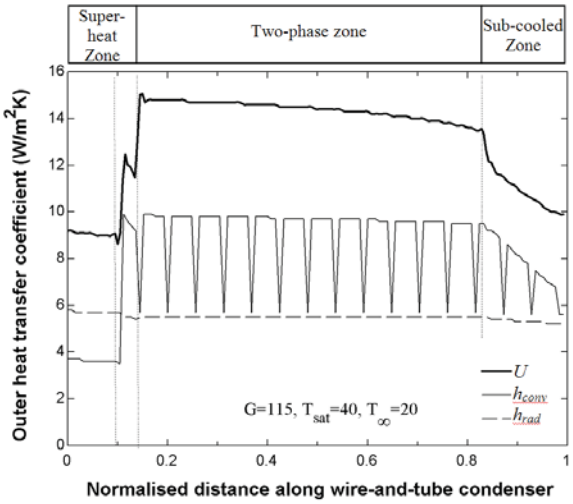

Figure 9: Variation of the heat transfer coefficients along W&T condenser

OPTIMISATION OF EVAPORATOR/CONDENSER

To find a more economical solution for an improved evaporator or condenser design for domestic refrigerators, Bansal et al. (2001) and Bansal and Chin (2003b) introduced a useful parameter called the optimisation factor, f_o. This relates the optimum heat exchanger design with its current maximum capacity per unit weight and is defined as the ratio:

$$f_o = \frac{\dot{Q}_{optimised}/w_{optimised}}{\dot{Q}_{100\%}/w_{100\%}} \quad (32)$$

An optimum design should ideally result in Q_{opt} to increase, while W_{opt} to decrease, yielding the f_o value to be greater than one.

Egg crate evaporator

The results of the optimum egg crate evaporator can be seen in Figure 10. Case I refers to the highest fin density, the

smallest fin height and the thickest fins. This lead to an increase in capacity of 14.5%, but it also increased the material weight of 70.5%. Applying the optimisation factor in equation (32), case II is the optimised egg crate evaporator, providing an increase in evaporator capacity by 4.7% while decreasing the material weight by 72%.

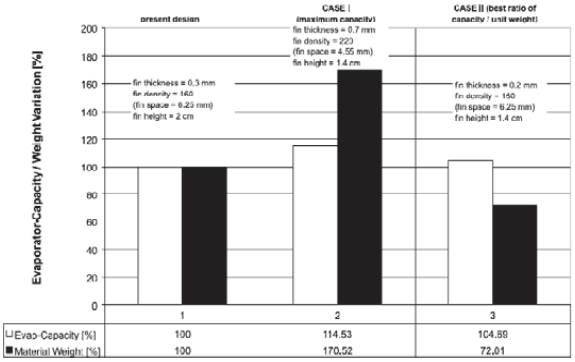

Figure 10: Optimisation of egg crate evaporator

Wire and tube condenser

The optimisation factor in equation (32) was also be applied by Bansal and Chin (2003b) for condenser design optimisation, where $f_o > 1$ is desired for better capacity per unit weight of the condenser.

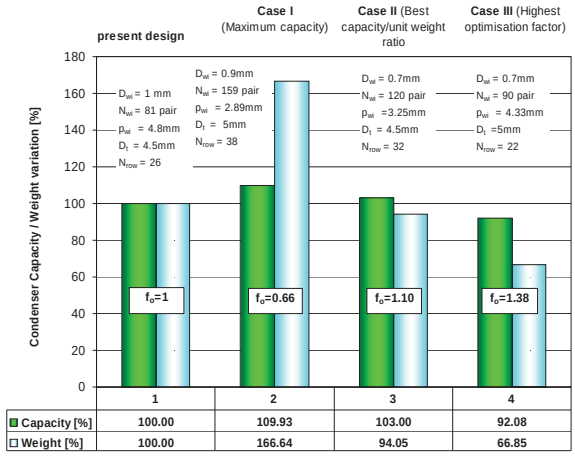

Figure 11: Optimisation of the wire-and-tube condenser

The optimisation process uses a combination of condenser density, diameter, tube diameter and tube pitch. Generally, the optimisation factor, f_o is higher for smaller condenser capacity. It deteriorates with higher condenser capacities due to increasing weight of the condenser. Three outcomes from the simulation results by Bansal and Chin (2003b) and are shown in Figure 11.

Maximum capacity is achieved for case I, with the maximum number of coils with the largest diameter of tubes. However, there is a significantly larger increase in the material weight and the optimisation factor is reduced. Case II is one which yields an increase in condenser capacity as well as a reduction in weight. Generally, increasing the fins diameter and tube and fin density can increase the capacity, consequence of that is an increase in weight. The largest optimisation factor is achieved in case III, where the condenser capacity is reduced faintly, and there is a very significant reduction in the weight. This optimised design is obtained using a smaller wire diameter, larger fins and tube density.

CONCLUSIONS

This paper has presented the physics and fundamentals of the two 'generic' heat exchanger modelling techniques, namely the LMTD and NTU-e, particularly when one of the streams is undergoing phase change. Subsequently, the paper presented their novel features, some of their salient differences, and their areas of application. The paper has highlighted the usefulness of NTU-e approach for heat exchangers undergoing phase change. Specific industrial examples of two novel heat exchangers were presented that were optimised for their use in domestic refrigerators. It is hoped that this paper will be helpful for designers and academia for implementing the modelling techniques in their applications.

ACKNOWLEDGEMENTS

The author is thankful to Mr Ossma Iqbal for his valuable assistance in preparing this paper.

NOMENCLATURE

A	Area [m^2]	*Subscripts*	
$\dot{C}$	Capacity rate [kJ/kg.K]	*a*	air
C_P	Specific heat [kJ/kg.K]	*ave*	average
C_R	Capacity ratio [-]	CO_2	Carbon dioxide
d	Tube diameter [m]	*e*	Evaporator
D_h	Hydraulic diameter [m]	*e1*	Element 1
f	Friction parameter [-]	*f*	Fouling
G	mass flux: [kg m^{-2}]	*HX*	Heat exchanger
h	Enthalpy [kJ kg^{-1}]	*i*	Inner tube wall
I_0	First modified zero-order Bessel function	*l*	Liquid
K_0	Second modified zero-order Bessel function	*lat*	Latent
k	Thermal conductivity [W/mK]	*max*	Maximum
L	Heat exchanger length [m]	*min*	Minimum
L_e	Lewis number [-]	*n1*	Node 1
m	Mass of frost [kg]	*o*	Outer tube wall
$\dot{m}$	Mass flow rate [kgs^{-1}]	*r*	Refrigerant
Nu	Nusselt number [-]	*s*	Secondary fluid / frost surface

NTU	Number of transfer units [-]	*sc*	Sub-cooling zone
ΔP	Change in Pressure [kPa]	*sen*	sensible
Pr	Prandtl number [-]	*SF*	Secondary fluid
$\dot{Q}$	Heat transfer rate [W]	*sg*	sublimation
R	Resistance [m^2KW^{-1}]	*sh*	Superheat zone
T	Temperature [K]	*tot*	Total
ΔT_{LMTD}	Log mean temperature difference [K]	*tp*	Two-phase zone
U	Overall heat transfer coefficient [W m^{-2} K^{-1}]	*v*	Vapour
x	Vapour quality [-]	*z*	Zone
Greek symbols			
α	Heat transfer coefficient [W m^{-2} K^{-1}]	σ	ratio of minimum flow area to face area[-]
ε	Effectiveness [-]	φ	fin efficiency
η	Surface efficiency [-]	ω	humidity ratio: [$kg.kg^{-1}$ dry air]
μ	dynamic viscosity: [kg m^{-1} s^{-1}]	ρ	density [$kg.m^{-3}$]

REFERENCES

Bansal, P.K., and Chin, T. 2003a. *Heat transfer characteristics of wire-and-tube and hot wall condensers*. International Journal of HVAC&R 9(3), pp. 277-290.

Bansal, P.K., and Chin, T. 2003b. *Modelling and optimisation of wire-and-tube condensers*. International Journal of Refrigeration 26(5), pp 601-613.

Bansal, P.K., Wich, T., Chen, J., and Browne, M.W. 2001. *Design and modelling of new-egg-crate type forced flow evaporators in domestic refrigerators*. ASHRAE Transactions, Paper no. 4474, 107 (2), pp 204 - 211.

Browne, M., and Bansal, P.K. 2001. *Different modelling strategies of in-situ liquid chillers*. Proc. Inst. Mech. Engrs. (UK), Part A, J Power and Energy, 215 (A3), pp 357 – 374.

Chapman, A.J. 1984. *Heat transfer, 4th Ed*. New York: Collier Macmillan.

Collier, J.G. and Thome, J.R.1994. *Convective boiling and condensation, 3rd Ed*. Oxford New York: Clarendon Press.

Domanski, P. A. And Yashar, D. 2007, *Application of an evolution program for refrigerant circuitry optimization*, Proc. ACRECONF- Challenges to Sustainability, Delhi (India).

Incropera, F.P., and DeWitt, D.P. 1990. *Fundamentals of Heat and Mass Transfer, 3rd Ed*. New York: John Wiley and Sons.

Getu, M., and Bansal, P.K. 2007. *Limitations of Frost properties correlations.* International Congress of Refrigeration, Beijing (China). August 21-27, 9 pages.

Getu, M., and Bansal, P.K. 2006. *Simulation model for a low-temperature supermarket refrigeration system*. International Journal of HVAC&R. 12(4), pp 1117 - 1139.

Iu, I., Weber, N., Bansal, P. K., and Fisher, D. 2007. *Applying the effectiveness-NTU method to the elemental heat exchanger models*, ASHRAE Transactions, **113**(1), 15 pages.

Iu, I., Bansal, P. K., Rees, S., Fisher, D. and Spitler, J. 2003. *Energy efficiency analysis of a unitary heat pump system*, Proc. International Conference on Building Systems and Facilities Management – Integrating Innovations and Technologies For a Built Environment, Singapore, October 8 – 10, pp 334 - 341.

Kays, W.M., and London, A.L. 1964. *Compact heat exchangers, 2nd ed*. New York: McGraw Hill.

Kim, N.H., Youn,B., and Webb, R.L. 1998. *Heat transfer and friction correlations for plain fin-and-tube heat exchangers. Heat transfer*. Proceedings of the 11th International Heat Transfer Conference, Kyongju, Korea: 209-213.

Seker, D., Karatas, H., and Egrican, N. 2004. *Frost formation on fin-and-tube heat exchangers. Part I: Modeling of frost formation on fin-and-tube heat exchangers*. International Journal of Refrigeration 27: 367-374.

Singh, V., Aute, V., and Radermaker, R. 2009. *A heat exchanger model for air-to-refrigerant fin-and-tube heat exchanger with arbitrary fin sheet*, International Journal of Refrigeration 32: 1724-1735.

Tao, Y.X., Besant, R.W., and Mao, Y. 1993. *A mathematical model for predicting the densification of frost on a flat plate*. Int J Heat Mass Transfer 2: 353-363.

Threlkeld, J.L. 1970. *Thermal environmental engineering, 2nd Ed. Englewood Cliffs*. NJ: Prentice Hall Book Co.